A&A 543, A98 (2012)
DOI: 10.1051/0004-6361/201219332

Astronomy & Astrophysics

The mass of the planet-hosting giant star β Geminorum determined from its p-mode oscillation spectrum⋆,⋆⋆

A. P. Hatzes[1], M. Zechmeister[2], J. Matthews[3], R. Kuschnig[4], G. A. H. Walker[5], M. Döllinger[1], D. B. Guenther[6], A. F. J. Moffat[7], S. M. Rucinski[8], D. Sasselov[9], and W. W. Weiss[4]

[1] Thüringer Landessternwarte Tautenburg, Sternwarte 5, 07778 Tautenburg, Germany
e-mail: artie@tls-tautenburg.de
[2] Georg-August-Universität Göttingen, Friedrich-Hund-Platz 1, 37077 Göttingen, Germany
[3] Department of Physics, University of British Columbia, 6224 Agricultural Road, Vancouver, BC V6T 1Z1, Canada
[4] Institut für Astronomie, Universität Wien Türkenschanzstrasse 17, 1180 Vienna, Austria
[5] 1234 Hewlett Place, Victoria, BC V8S 4P7, Canada
[6] Institute for Computational Astrophysics, Department of Astronomy and Physics, Saint Mary's University, Halifax, NS B3H 3C3, Canada
[7] Observatoire Astronomque du Mont Mégantic, Départment de Physique, Université de Montréal C.P. 6128, Succursale: Centre-Ville, Montréal, QC H3C 3J7, Canada
[8] Department of Astronomy and Astrophysics, University of Toronto, Toronto, ON M5S 3H4, Canada
[9] Harvard-Smithsonian Center for Astrophysics, 60 Garden Street, Cambridge, MA 102138, USA

Received 3 April 2012 / Accepted 21 May 2012

ABSTRACT

Aims. Our aim is to use precise radial velocity measurements and photometric data to derive the frequency spacing of the p-mode oscillation spectrum of the planet-hosting star β Gem. This spacing along with the interferometric radius for this star can then be used to derive an accurate stellar mass.

Methods. We use a long time series of over 60 h of precise stellar radial velocity measurements of β Gem taken with an iodine absorption cell at the echelle spectrograph mounted on the 2 m *Alfred Jensch* Telescope. We also present complementary photometric data for this star taken with the MOST microsatellite spanning 3.6 d. A Fourier analysis is used to derive the frequencies that are present in each data set.

Results. The Fourier analysis of the radial velocity data reveals the presence of up to 17 significant pulsation modes in the frequency interval 10−250 μHz. Most of these fall on a grid of equally-spaced frequencies having a separation of 7.14 ± 0.12 μHz. An analysis of 3.6 days of high precision photometry taken with the MOST space telescopes shows the presence of up to 16 modes, six of which are consistent with modes found in the spectral (radial velocity) data. This frequency spacing is consistent with high overtone radial pulsations; however, until the pulsation modes are identified we cannot be sure if some of these are nonradial modes or even mixed modes. The radial velocity frequency spacing along with angular diameter measurements of β Gem via interferometry results in a stellar mass of $M = 1.91 \pm 0.09\ M_{\odot}$. This value confirms the intermediate mass of the star determined using stellar evolutionary tracks.

Conclusions. β Gem is confirmed to be an intermediate mass star. Stellar pulsations in giant stars along with interferometric radius measurements can provide accurate determinations of the stellar mass of planet hosting giant stars. These can also be used to calibrate stellar evolutionary tracks.

Key words. techniques: radial velocities – stars: individual: β Geminorum – stars: late-type

1. Introduction

There are several programs underway that use precise stellar radial velocity (RV) measurements to search for planets around evolved giant stars (e.g. Setiawan et al. 2003; Sato et al. 2003; Johnson et al. 2007; Niedzielski et al. 2009; Han et al. 2010). The reason is that the progenitors of these giant stars are A-F dwarfs – stars that have high effective temperatures and rapid rotation rates that makes it almost impossible to detect the subtle reflex motion from any planetary companion with RV measurements. Although giant stars offer us a means of detecting planetary companions around stars more massive than the sun, there is a drawback in the determination of an accurate stellar mass. Unlike for main sequence stars that have a tight and reasonably well calibrated relationship between stellar mass and effective temperature, the evolutionary tracks of giants stars covering a broad range of stellar masses all converge to the same region of the H-R diagram. One must rely on evolutionary

⋆ Based on observations obtained at the 2 m Alfred Jensch Telescope at the Thüringer Landessternwarte Tautenburg and data from the MOST satellite, a Canadian Space Agency mission, jointly operated by Dynacon Inc., the University of Toronto Institute of Aerospace Studies and the University of British Columbia with the assistance of the University of Vienna.

⋆⋆ Tables of the radial velocities and photometric measurements are only available at the CDS via anonymous ftp to cdsarc.u-strasbg.fr (130.79.128.5) or via http://cdsarc.u-strasbg.fr/viz-bin/qcat?J/A+A/543/A98

tracks, which are model dependent and require accurate stellar parameters (luminosity, effective temperature, abundance, etc.), to determine the stellar mass. Accurate stellar masses of planet hosting giant stars are needed if we are to understand the process of planet formation as a function of stellar mass.

The bright star β Gem is a planet-hosting K giant star (Hatzes & Cochran 1993; Hatzes et al. 2006; Reffert et al. 2006) that was recently shown to exhibit stellar oscillations. Hatzes & Zechmeister (2007, hereafter HZ07) using 20 h of precise stellar radial velocity measurements demonstrated that this star shows up to 6 oscillation modes in the frequency range $\nu = 10-150$ μHz. The most dominant mode was at $\nu = 89$ μHz and had an amplitude of 5 m s^{-1}. The pulsation frequencies and amplitudes were consistent with those expected for solar-like p-mode oscillations for a giant star with radius $R = 8.8\ R_{\odot}$ and mass, $M \approx 2\ M_{\odot}$. The former was determined from interferometric measurements (Nordgren et al. 2001).

The mass estimate of β Gem by HZ07 was based on the frequency of maximum power, $\nu_{\rm max}$, and the scaling relations of Kjeldsen & Bedding (1995). This is not as accurate for two reasons. First, using a short time span of data (3 nights in the case of HZ07) we cannot be sure that the dominant mode we detect accurately represents $\nu_{\rm max}$. Likewise fitting a Gaussian to the envelope of observed excess power may have a large error. Second, to derive the mass from $\nu_{\rm max}$ one requires a knowledge of the effective stellar temperature which is not well constrained. On the other hand, the stellar mass determined from the frequency spacing depends only on the stellar radius (measured with interferometry in this case) and is thus independent of other more poorly determined stellar parameters like temperature or surface gravity. If one knows the stellar radius, one can thus derive the stellar mass. Just as important, determining the precise frequencies of as many detected modes as possible and their separation are more valuable for asteroseismic modeling than just determining $\nu_{\rm max}$. Unfortunately, the data set of HZ07 was of insufficient length to do this.

In this paper we use a much larger data set with over 60 h of coverage, including the measurements presented in HZ07, to derive the oscillation spectrum and thus the frequency spacing of β Gem. We also present photometric observations taken with the MOST space telescope.

2. Observational data

2.1. Spectral data

Radial velocity measurements were made using the coude echelle spectrograph of the 2 m *Alfred Jensch* Telescope of the Thüringer Landessternwarte Tautenburg (Thuringia State Observatory). Observations were made on 10 nights over the time span 24 December 2006 to 18 April 2007, or a difference of 116 days from first to last observation. A total of over 60 h of observations were made resulting in over 762 measurements. Precise stellar radial velocities were determined using an iodine absorption cell placed in the optical path of the telescope. A further description of the instrumental setup and RV analysis method can be found in Hatzes et al. (2005). Table 1 lists the journal of observations.

The planetary companion to β Gem causes a reflex motion of 39 m s^{-1} with a period of 590 days. This orbital motion was removed and the subsequent analysis performed on the residual RV data. Figure 1 shows the RV measurements for 9 of the nights after removal of the orbital motion. Figure 2 shows the residual RVs after subtracting the fit discussed in more detail below.

Table 1. Journal of observations.

Start (Julian Day)	Time coverage (h)	$N_{\rm Obs}$	σ (m s^{-1})
2 450 076.650	2.16	38	1.65
2 450 077.491	4.70	58	1.51
2 450 096.269	11.38	135	1.81
2 450 097.266	2.54	24	1.86
2 450 126.314	9.70	104	1.64
2 450 168.308	6.88	115	1.39
2 450 170.266	5.04	74	2.00
2 450 171.259	8.64	152	1.94
2 450 191.371	4.34	62	2.64
2 450 192.277	6.52	39	3.13

Notes. The table includes Julian date as the start of the night, time coverage per night, number of observations each night, and the rms scatter of the data about the multi-component frequency fit (see text).

In order to make a more compact figure for easy viewing we do not show the last night which was also included in our analysis. Although the time span of the observations (time between first and last data point) for this night is large compared to the other nights, there were large gaps and only 39 measurements were made due to poor observing conditions. Also, because of these conditions the RV precision was about a factor of 2 worse than the other nights. If we exclude these measurements the following results are not significantly altered.

2.2. Photometric data

Photometric measurements were taken using the Microvariability and Oscillations of Stars Microsatellite (MOST) space mission as part of a secondary observational program. MOST is 15/17.3 cm Rumak-Maksutov telescope with a CCD photometer in a circular Sun-synchronous polar orbit with a period of 101.41 min (Walker et al. 2003). MOST observed β Gem on 5 consecutive nights spanning 13−17 February 2007 (JD = 2 454 145.633 and 2 454 149.26). Individual exposures were set to 1.5 s and 14 images were stacked on board before downloading the data. Observations of β Gem alternated with those of a primary program of MOST. β Gem was continuously observed for 40 min followed by a gap of approximately 1 h for a duty cycle of about 40%. A total of 4440 photometric measurements were made of β Gem

Figure 3 shows the time series of the photometric measurements. For clarity data points shown in the figure are average values of 4 measurements (50 s).

3. Stellar parameters

β Gem is a nearby K0 III star at a Hipparcos-measured distance of 10.3 pcs (van Leeuwen 2007). The most recent interferometric measurements for this star yielded an angular diameter of 7.96 ± 0.09 mas (Nordgren et al. 2001) which corresponds to a radius of 8.8 ± 0.1 $R_{\odot}$.

This star has also been the subject of several spectral investigations. McWilliam (1990) measured an effective temperature, $T_{\rm eff}$, of 4850 K, a metalicity of [Fe/H] = −0.07, and a surface gravity, $\log g = 2.96$. Gray et al. (2003) derived the same effective temperature, but a lower surface gravity ($\log g = 2.52$), and higher metalicity ([Fe/H] = 0.08). Allende Prieto et al. (2004) determined $T_{\rm eff} = 4666 \pm 95$ K, a surface gravity of $\log g = 2.685 \pm 0.09$ and a metalicity [Fe/H] = 0.19.

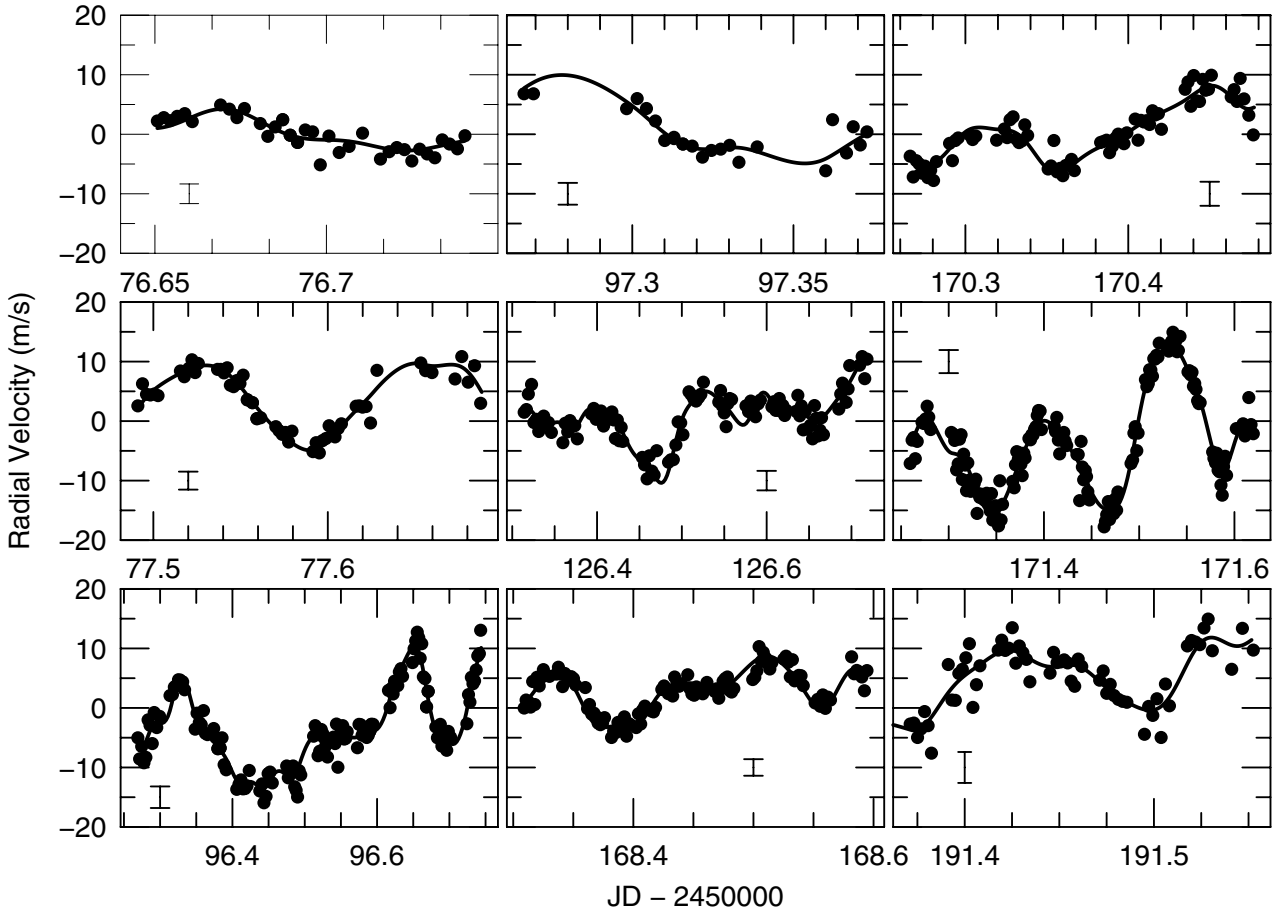

Fig. 1. Radial velocity measurements for β Gem on 9 different nights. The error bar in each panel shows the typical error for each night. The solid line represents the fit to the data using the frequencies and amplitudes in Table 2. For clarity we used variable limits for the ordinate.

Table 2. Pulsation frequencies from the RV data.

Mode	ν (c d^{-1})	ν (μHz)	Amp (m s^{-1})	FAP
f_{v1}	0.8675 ± 0.0001	10.03	5.39 ± 0.12	$<10^{-5}$
f_{v2}	7.5427 ± 0.0001	87.24	4.31 ± 0.10	$<10^{-5}$
f_{v3}	2.6971 ± 0.0002	31.20	2.92 ± 0.11	$<10^{-5}$
f_{v4}	8.0404 ± 0.0001	93.02	3.99 ± 0.12	$<10^{-5}$
f_{v5}	0.6806 ± 0.0002	7.87	2.35 ± 0.14	$<10^{-5}$
f_{v6}	9.9971 ± 0.0002	115.66	2.03 ± 0.12	$<10^{-5}$
f_{v7}	4.5330 ± 0.0002	52.41	2.48 ± 0.11	$<10^{-5}$
f_{v8}	6.9571 ± 0.0003	80.49	1.99 ± 0.11	$<10^{-5}$
f_{v9}	3.1520 ± 0.0005	36.47	1.05 ± 0.11	$<10^{-5}$
f_{v10}	11.3124 ± 0.0003	130.88	1.50 ± 0.11	$<10^{-5}$
f_{v11}	16.8300 ± 0.0005	194.72	0.98 ± 0.11	$<10^{-5}$
f_{v12}	12.4984 ± 0.0006	144.61	0.79 ± 0.10	$<10^{-5}$
f_{v13}	6.1863 ± 0.0005	71.58	1.05 ± 0.11	0.00001
f_{v14}	1.5158 ± 0.0006	17.54	0.90 ± 0.11	0.00016
f_{v15}	17.9305 ± 0.0006	207.46	0.87 ± 0.11	0.0074
f_{v16}	21.7746 ± 0.0006	251.93	0.65 ± 0.10	0.0164
f_{v17}	17.5591 ± 0.0008	203.16	0.63 ± 0.10	0.0197

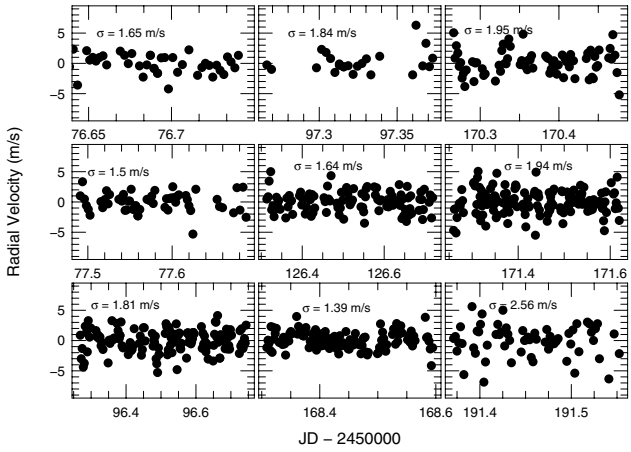

Fig. 2. Residual radial velocities after subtracting the fit using the frequencies and amplitudes in Table 2. In each panel the rms scatter for that night is given.

We also derived the stellar parameters for β Gem using a high signal-to-noise spectrum taken with the coude echelle spectrograph of the 2 m telescope at Tautenburg. Our analysis yielded $T_{\rm eff}$ = 4835 ± 50 K, $\log g$ = 2.70 ± 0.10, and [Fe/H] = −0.07 ± 0.05. These values are consistent with the McWilliam and Gray et al. values, and are in good agreement with the Allende Prieto et al. values with the exception that our analysis does not indicate such a high metalicity.

The stellar parameters of mass, radius, and age were determined using the online tool from Girardi (http://stev.oapd.inaf.it/cgi-bin/param). This tool uses a a library of theoretical isochrones (Girardi et al. 2000) and a modified version of the Baysian estimation method implemented by Jørgensen & Lindegren (2005). A detailed description of this method is given by da Silva et al. (2006). As input one needs the visual magnitude V, the parallax π, the effective temperature $T_{\rm eff}$, and the metalicity [Fe/H]. For the $T_{\rm eff}$ and the metalicity we used our derived

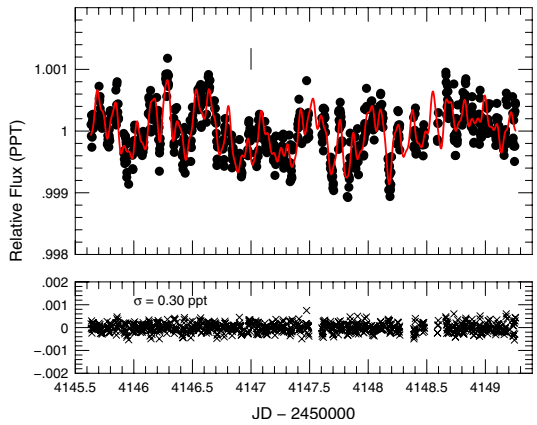

Fig. 3. (*Top*) Photometry of β Gem taken with the MOST microsatellite. The solid line represents the fit to the data using the frequencies and amplitudes in Table 4. (*Bottom*) Residuals after subtracting the fit. Units are in parts per thousand (PPT).

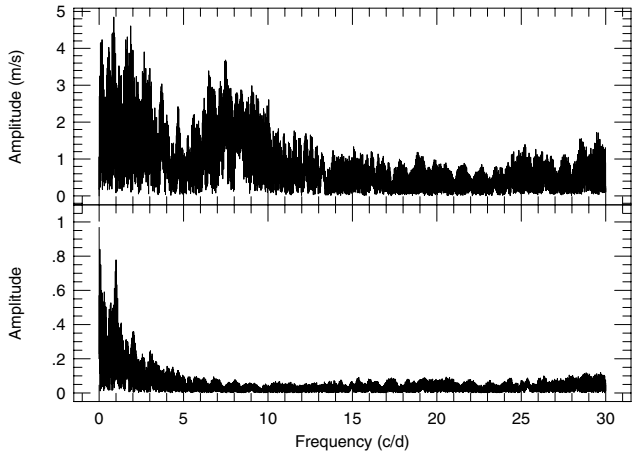

Fig. 4. (*Top*) The amplitude spectrum for the RV data. (*Bottom*) the window function.

values. The tool yields a stellar mass of $M = 1.96 \pm 0.19\ M_{\odot}$, an age of 1.19 ± 0.3 Gyr, and a radius of $R = 8.29 \pm 0.35\ R_{\odot}$. The radius is in very good agreement with the one derived from interferometric measurements. The stellar mass is also consistent with the frequency of maximum power for the oscillations observed by HZ07.

4. Frequency analysis

4.1. The RV data

A frequency analysis was done on the full RV data set using the program *Period04* (Lenz & Breger 2004) which performs a discrete Fourier transform on the data and then fits the time series with the found frequencies. We are aware that the oscillations in a giant star may not be coherent over the long time span of our observations. However, as a first analysis we wanted to see if a multi-component since function could adequately fit the data, and more importantly if the derived frequencies had a physical interpretation. The time unit for our RV analysis program is days, therefore frequency is expressed in c d^{-1}. In tables we also give the frequency in the more common units of μHz. Figure 4 shows the discrete Fourier transform amplitude spectra for the full data set as well as the spectral window. There appears to be excess power in two frequency ranges: 0.5−3 c d^{-1} and 6−10 c d^{-1}. The highest peak in the first frequency range is at 0.86 c d^{-1} and for the second range at 7.54 c d^{-1}. The latter corresponds to the dominant frequency found by HZ07 based on an analysis of a subset of the data presented here.

Table 3. Comparison of frequencies found in this work and HZ07.

HZ07 frequency (μHz)	This Work (μHz)	Comment
29.75 ± 0.54	31.20	
48.41 ± 1.06	36.47	1-day alias
79.47 ± 0.76	80.49	
86.91 ± 0.37	87.24	
104.40 ± 0.49	115.66	1-day alias
149.25 ± 0.63	144.61	1-day alias + $\Delta\nu_0$
193.63 ± 3.07	194.72	

In order to search for multiple modes we used the standard pre-whitening procedure. A Fourier transform of the data yielded the highest peak in the interval $0 < \nu < 30$ c d^{-1}. A least squares sine fit to the data was made with *Period04* using this frequency and its contribution was subtracted from the data. A Fourier analysis was then performed on the residuals to find the next dominant frequency in the data. This process was continued until no additional significant peaks were found. Finally, *Period04* was used to find a solution by fitting all sine components simultaneously.

In all cases the highest peak in the amplitude spectra was chosen at each step of the pre-whitening procedure. We are aware that the spectral window, noise, finite lifetime of pulsation modes, etc. can cause spectral leakage and the identification of a spurious pulsation mode. Rather than making a priori judgments as to which peak is real based on a preliminary frequency spacing of modes (see below) we simply chose the strongest peak. This may result in some of our identified modes being an alias frequency or the presence of artifact frequencies due to finite mode lifetimes.

Our analysis found a total of 17 significant frequencies in the RV time series. These are listed in Table 2 (denoted $f_{v1} - f_{v17}$) in the order in which they were found by the pre-whitening process. The line in Fig. 1 shows the fit to the RV data using these 17 modes and Fig. 2 shows the residual RV variations after subtracting the 17-component fit. The final rms scatter of the data about this fit is 1.9 m s^{-1} for the full data set. The rms scatter of the data about the final fit for each night is listed in Table 1. In their analysis of the nights 6−8 HZ07 obtained slightly better fits with rms scatter of 1.2, 1.5, and 1.7 m s^{-1}, for each night respectively. The slightly poorer rms scatter when fitting the entire data set may be due to amplitude variations in the different modes over the time span of the measurements (116 days) or due to mode lifetimes shorter than the full time span of our observations. If the time scales of these possible amplitude variations are of ≈days, then fitting subsets of the data should result in better fits. The white noise level was estimated using *Period04* in the frequency range $\nu = 10$−30 μHz (0.86−2.59 c d^{-1}) and after subtracting the contribution of the found modes. This level was ≈0.15 m s^{-1}.

The statistical significance of the periods were assessed using a "bootstrap randomization technique" (see Kürster et al. 1999). After removing the previous dominant frequency the RV values were randomly shuffled keeping the times fixed and a Scargle periodogram calculated (Scargle 1982). A Scargle periodogram was used since the power is a measure of the statistical significance of a signal. After a large number of

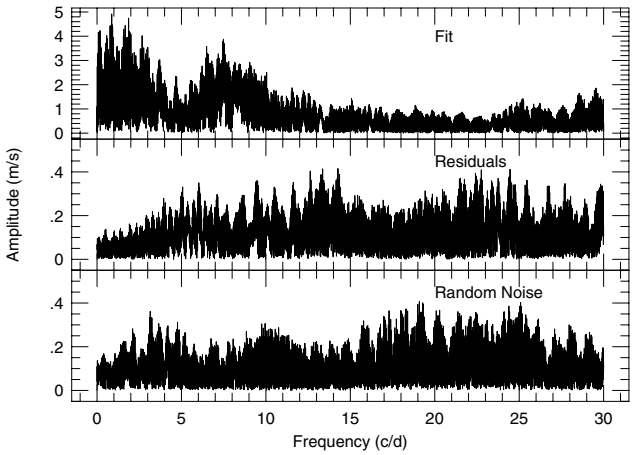

Fig. 5. (*Top*) The amplitude spectrum of the 17-component fit to the data that was sampled in the same manner as the data. Random noise with $\sigma = 2$ m s^{-1} was also added to the synthetic data. (*Middle*) The amplitude spectrum of the residual RVs after subtracting the fit to the data. (*Bottom*) The amplitude spectrum of random noise with $\sigma = 2$ m s^{-1} that was sampled in the same manner as the data.

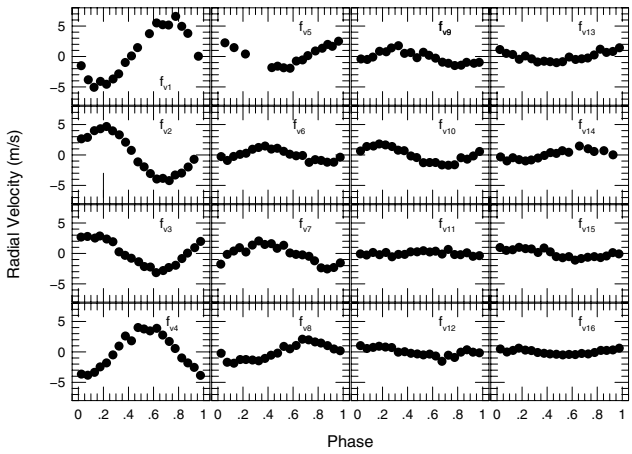

Fig. 6. Phase diagrams showing the residual RV measurements phase to the frequencies found in the Fourier analysis. For each panel the contribution of all other frequencies were subtracted prior to phasing the data. Data were phased in phase bins of 0.05. The gap in panel $f_{\upsilon 5}$ is an artifact of the sampling and frequency.

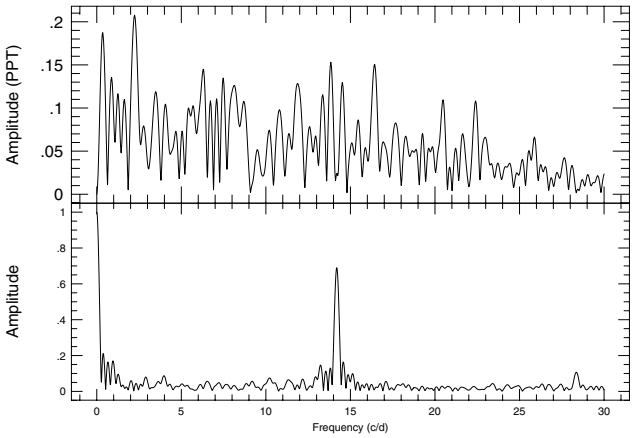

Fig. 7. (*Top*) DFT amplitude spectrum of the MOST photometric data. Units are in parts per thousand (PPT). (*Bottom*) the window function. The peak at 14.2 c d^{-1} seen in the window function is due to gaps in the data (see text).

shuffles (100 000) the fraction of random periodograms having Scargle power greater than the data periodogram gave an estimate of the false alarm probability (FAP), that is the probability that a signal was due purely to noise possibly in combination with the spectral window. The FAPs are also listed in Table 2. FAPs with upper limits indicate that there was no instance in 100 000 random data sets where the power of the Scargle periodogram exceeded the data periodogram. The first 12 frequencies found by our pre-whitening procedure are highly significant having FAP $< 10^{-5}$. Frequencies $f_{13} - f_{15}$ are also very significant having FAPs well below 1%. The final two frequencies are moderately significant with FAP $\approx$2% however, since these fall near the derived frequency spacing (see below) they may indeed be real.

We compared the amplitude spectrum of the 17-component fit to that of the observed amplitude spectrum. The top panel in Fig. 5 shows the amplitude spectrum of the 17-component fit to data using the frequencies and amplitudes of Table 2 and sampled in the same manner as the data. Random noise with $\sigma = 2$ m s^{-1} was also added to the data. The middle panel of Fig. 5 shows the amplitude spectrum of the final residuals of the data after removing the 17-component fit. The bottom panel in the figure shows the amplitude spectrum of pure noise with a standard deviation of 2.0 m s^{-1} that was sampled in the same manner as the data.

There are several things to note about this figure. First, the synthetic fit with noise has an amplitude spectrum that is similar to the data spectrum. A 17-component sine function with the proper sampling and noise can adequately reproduce most of the features seen in the amplitude spectrum. Second, the amplitude spectrum of the final residuals also looks similar to the spectrum of random noise. Finally, much of the structure seen in the data amplitude spectrum at 0.3−3 c d^{-1} and 6−10 c d^{-1} (top panel Fig. 4) cannot be due to white noise combined with the spectral window.

We now compare the results of our frequency analysis to those of HZ07 whose analysis was based only on a three-night subset of the data presented here. HZ07 found evidence for seven modes in the data and these are listed in Table 3. This table also lists the nearest frequencies found by the current analysis. Four of the modes found by an analysis of the full data set coincide within the errors to peaks found by HZ07. Two other modes (48.41 μHz and 36.47 μHz) found by HZ07 are most likely 1-day aliases of the true frequency. The 149.3 μHz mode found by HZ07 may be an alias of 137.68 μHz. This mode differs by 6.8 μHz from a mode found by the current analysis. This difference is close to the frequency spacing, $\Delta\nu$, found in this work (see below). In conclusion, the frequencies found by HZ07 on the limited subset of data are for the most part consistent with those found by an analysis of the full data set.

Figure 6 shows the phase diagram of the RV variations from the individual modes found in our frequency analysis. For each displayed frequency the contribution of the other modes was first removed before phasing the data. For clarity we display phase-averaged values using bins of 0.05 in phase. Note that the phase gap in the panel for $f_{\upsilon 5}$ is an artifact of the sampling and phasing the data to this frequency.

4.2. MOST photometry

A period analysis was also performed on the MOST photometry. Figure 7 shows the discrete Fourier transform of the MOST data and the spectral window. The white noise in the DFT estimated

Table 4. Pulsation frequencies derived from MOST photometry.

Mode	ν ($c\,d^{-1}$)	ν (μHz)	Amp (PPT)	FAP
f_{p1}	2.11 ± 0.01	24.41 ± 0.12	0.180 ± 0.013	$<10^{-5}$
f_{p2}	0.38 ± 0.01	4.40 ± 0.14	0.167 ± 0.012	$\approx 10^{-4}$
f_{p3}	6.34 ± 0.01	73.35 ± 0.12	0.142 ± 0.010	$\approx 10^{-5}$
f_{p4}	7.50 ± 0.01	86.77 ± 0.12	0.123 ± 0.009	$\approx 10^{-5}$
f_{p5}	8.79 ± 0.01	101.70 ± 0.13	0.106 ± 0.011	0.002
f_{p6}	11.41 ± 0.02	132.01 ± 0.20	0.078 ± 0.017	0.002
f_{p7}	8.18 ± 0.01	94.64 ± 0.15	0.120 ± 0.013	0.002
f_{p8}	3.39 ± 0.01	39.22 ± 0.16	0.115 ± 0.014	0.002
f_{p9}	4.09 ± 0.01	47.32 ± 0.11	0.122 ± 0.010	0.002
f_{p10}	0.88 ± 0.01	10.18 ± 0.14	0.138 ± 0.012	0.007
f_{p11}	2.36 ± 0.03	27.30 ± 0.29	0.132 ± 0.025	0.003
f_{p12}	7.04 ± 0.02	81.45 ± 0.23	0.075 ± 0.020	0.002
f_{p13}	1.69 ± 0.02	19.55 ± 0.26	0.089 ± 0.023	0.027
f_{p14}	1.27 ± 0.02	14.69 ± 0.20	0.093 ± 0.017	0.010
f_{p15}	17.84 ± 0.02	206.40± 0.20	0.072 ± 0.017	0.021
f_{p16}	9.57 ± 0.02	110.72 ± 0.23	0.058 ± 0.020	0.010

Notes. Amplitudes are in parts per thousand (PPT).

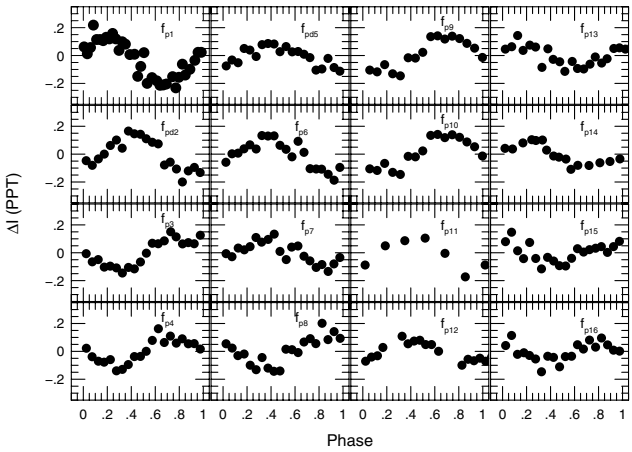

Fig. 8. Phase diagrams showing the residual photometric measurements phased to the frequencies found in the Fourier analysis. For each panel the contribution of all other frequencies were subtracted prior to phasing the data. Data were phased in phase bins of 0.05 except for f_{p11} where a bin of 0.1 was used.

at frequencies above 30 $c\,d^{-1}$ was about 0.025 parts per thousand (PPT). The pre-whitening procedure was applied until all frequencies with amplitudes greater than four times the noise level were found. These correspond to false alarm probabilities less than 0.01. A total of 16 frequencies were found which are listed in Table 4 (denoted $f_{p1} - f_{p16}$). Also listed are the false alarm probabilities calculated using the same procedure as for the RV measurements and 100 000 shuffles of the data. The final RMS scatter of the data about the fit is 0.13 PPT.

At least six of the photometric frequencies have counterparts in the RV data. The highest amplitude photometric modes at 2.11 and 0.38 $c\,d^{-1}$ appear to have no counterparts in the RV data. However, we caution the reader that a number of effects make a direct comparison to the RV frequencies difficult: 1) The RV data are more effected by alias effects than the photometric data. 2) The spectroscopic and photometric data were not contemporaneous and the spectroscopic data in particular were taken over a larger time span. 3) The photometric amplitudes detected by MOST were small and the time span of the MOST observations were relatively short for the detection of such modes. A more reliable detection of photometric modes may require a more extended MOST observing run. In spite of these caveats, it is clear that several of the same oscillation frequencies are seen in both data sets.

Figure 8 shows the phase diagrams of the individual photometric modes. As in the case for the RV figure the contribution of all the other frequencies were first removed before phasing the data. For clarity we averaged the data in bins of 0.05 in phase. In some cases the frequency and the sampling resulted in a natural "clumping" of points which dictated a different binning of the data (e.g. f_{p11}).

5. The p-mode oscillation spectrum

The top panel of Fig. 9 shows the schematic of the RV oscillation spectrum (amplitudes and frequencies) as solid lines. The frequency range 70−100 μHz seems to show modes that are equally-spaced in frequency with a spacing of ≈10 μHz However, not all the detected modes seem to follow this spacing. We suspect that this may be either due to "missing modes" that were not detected either because they have too low an amplitude, were simply not present, or could not be detected due to the sampling of our data.

Since we are most likely dealing with p-mode oscillations it is reasonable to expect that the modes are evenly spaced in frequency. We tried to find a mean frequency spacing that could fit the observed spacing. We took the dominant mode at 87.24 μHz as our "origin" and calculated a set of predicted frequencies according to $\nu = \nu_0 \pm n\Delta\nu$, where $\nu_0 = 87.24$ μHz and n an integer. Thus the modes on either side of ν_0 will have $n = \pm 1$, ± 2, ..., etc. A value of n was chosen so that the predicted mode was as near as possible in frequency to the observed modes. A frequency spacing $\Delta\nu$ was then found that minimized the differences between the observed and predicted frequencies.

The dashed lines show the location of the predicted frequencies using a frequency spacing of $\Delta\nu = 7.14$ μHz. Most modes fit extremely well on this frequency spacing with the possible exception of the lowest frequency modes. This is not surprising since only high order modes should have an evenly-spaced frequency separation. The rms scatter of the observed minus fitted frequencies (O−C) is 0.38 μHz. Approximately 11 modes were used to derive the frequency spacing, so we adopt a value of $0.38/\sqrt{10}$ μHz = 0.12 μHz as the error in the frequency spacing determination.

The bottom panel of Fig. 9 shows the schematic of the photometric oscillation spectrum derived from the MOST photometry. Again we tried to find a mean frequency separation using the same procedure as the RV data. This resulted in a frequency spacing for the photometric modes with $\nu > 60$ μHz of $\Delta\nu = 7.07 \pm 0.32$ μHz consistent with the value determined from the RV data. The grid shows the location of the predicted frequencies found from the RV measurements.

6. The Mass of β Gem

The large separation of p-modes are given by

$$\nu_{n,\ell} \approx \Delta\nu_0(n + \ell/2 + \delta\nu)$$

where n and ℓ are the order and degree of the modes, and $\delta\nu$ is the small spacing that is related to the stellar structure (Tassoul 1980). If the modes are non-radial then the observed frequency spacing is just one-half of the large spacing. If the modes are

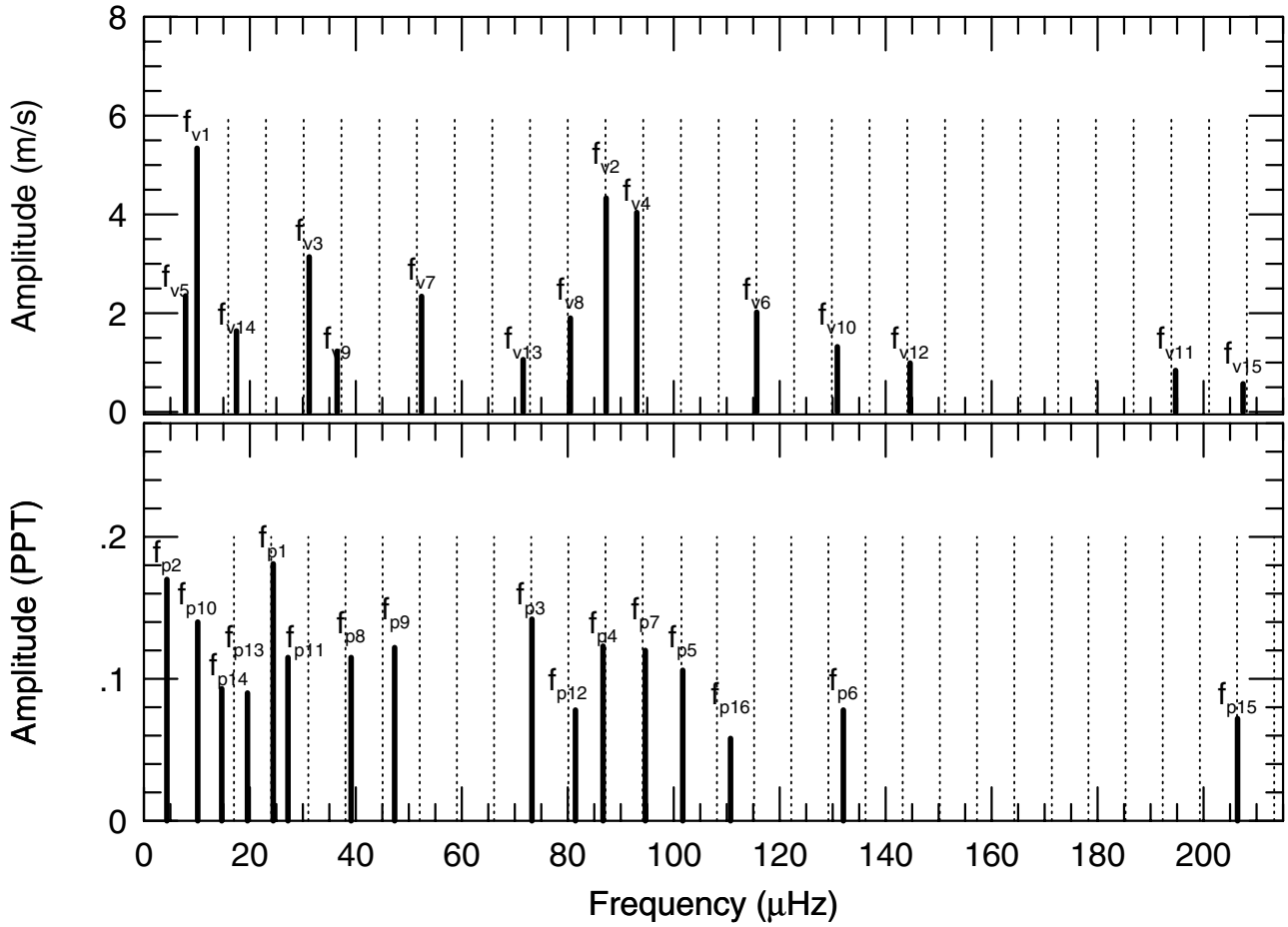

Fig. 9. Schematic of the oscillation spectrum for β Gem based on the RV measurements (*top*) and *MOST* photometry (*bottom*).

radial ($\ell = 0$) then the large spacing is the observed frequency spacing.

This large separation is related to the mean density of the star by

$$\Delta\nu = 135\,(M/M_\odot)^{0.5}\,(R/R_\odot)^{-1.5}\ \mu\text{Hz}.$$

Assuming that these are all radial modes ($\ell = 0$), the spacing of 7.14 ± 0.12 μHz and the measured radius of $R = 8.8 \pm 0.1\ R_\odot$ results in a stellar mass of $M = 1.91 \pm 0.09\ M_\odot$. Using the spacing found in the photometric data results in $M = 1.88 \pm 0.09\ M_\odot$. A more precise mass determination requires asteroseismic modeling of the observed frequency spectrum.

According to the scaling relationships the frequency of maximum power, $\nu_{\rm max}$, is also related to the mass and radius of the star. From Kjeldsen & Bedding (1995):

$$\nu_{\rm max} = M/R^2\,\sqrt{T_{\rm eff}/5777\ \text{K}}\ 3.05\ \mu\text{Hz}$$

where M, and R are in solar units. So, in principle one can determine the mass and radius of the star from $\nu_{\rm max}$ and $\Delta\nu$ alone. For the case of β Gem, $\nu_{\rm max} = 0.087$ mHz (ignoring low frequency modes) and $\Delta\nu = 7.14\ \mu$Hz. This results in $R = 9.3\ R_\odot$ and $2.25\ M_\odot$, in good agreement with the interferometric radius and subsequent mass determination.

We should note that these scaling relations were derived from solar type stars, but seem to hold also for evolved red giant stars (Kallinger et al. 2009; Stello et al. 2009). Also, recent results from the Kepler Mission indicate that K giants can have mixed $\ell = 1$ modes (Mosser et al. 2012) which can shift the observed frequencies. We cannot say from our data whether β Gem has such modes or whether we could have detected them with our RV measurements. If present they may affect the accuracy of frequency spacing determination.

7. Discussion

Our long time series of precise RV measurements for β Gem reveals the clear presence of p-mode oscillations in this star. These frequencies fall on a grid of equally-spaced frequency on an interval of $\Delta\nu = 7.14 \pm 0.2\ \mu$Hz. Photometric measurements taken with the MOST micro-satellite also show a comparable frequency spacing. Most of the photometric mode match up well with those detected in the spectroscopy.

It seems that these modes must be high overtone radial modes ($\ell = 0$). Nonradial modes would have a large spacing of twice the observed frequency spacing or ≈14 μHz. This implies a stellar mass $M \approx 8\ M_\odot$ which would be greatly at odds with stellar evolutionary tracks.

There is evidence that K giant stars can exhibit *both* radial and nonradial modes. Hatzes & Cochran (1994) suggested that the short-period RV variations in α Boo were consistent with fundamental or low-overtone radial modes. Buzasi et al. (2000) reported the detection of 10 modes in α UMa using the guide camera of the failed WIRE satellite. These were spaced on frequency interval of 2.94 μHz which was consistent with overtone radial pulsations. Radial modes have also been claimed for ϵ Oph (De Ridder et al. 2006) using RV measurements. Barban et al. (2007) observed this star photometrically with MOST and detected 7 equidistant peaks that were interpreted as radial modes.

Table 5. Ratio of RV to photometric amplitude of modes found in β Gem.

ν_{RV} (μHz)	Amp_{RV} (m s^{-1})	ν_{Phot} (μHz)	Amp_{Phot} (milli-mag)	2 K/Δm (km s^{-1} mag^{-1})
80.49	2.00	81.45	0.075	53 ± 14
87.24	4.31	86.77	0.123	70 ± 5
93.02	4.00	94.64	0.112	71 ± 6
10.03	5.39	10.18	0.138	78 ± 8
71.58	1.05	73.35	0.140	15 ± 7
130.88	1.50	132.01	0.078	38 ± 14

However, this result was not without dispute. Kallinger et al. (2008) re-examined the available data on ϵ Oph and argued for the presence of 21 modes. They were able to match these modes with a model that included both radial and non-radial modes. The unequivocal detection of both radial and non-radial modes finally came from light curves from the CoRoT space telescope. De Ridder et al. (2009) examined light curves from giant stars from the first long run of 150 days (LRc01) from CoRoT and found strong evidence for the presence of radial and nonradial modes, particularly in the star CoRoT-101034881. However, Baudin et al. (2012) used 60-d of CoRoT observations of the giant star HD50890 and found oscillations between 10−20 μHz that were consistent with a regular spacing of 1.7 μHz consistent with *only* radial modes. So it may be that some giant stars can oscillate in predominantly radial modes and others with both modes. (Of course the stars with pure radial pulsations may also possess non-radial modes that are simply not detected.)

There is some evidence for nonradial modes, at least in the photometric data. For instance, f_{p14}, f_{p15} and possibly f_{p9} may lie on the half interval of the large spacing derived from what we think are radial modes. Nonradial modes may well exist in β Gem, but possibly were not detected because of their low RV amplitudes and/or because of our limited time coverage. Furthermore, until the modes are actually identified some of the ones shown in Fig. 9 may in fact be nonradial modes.

Evidence for the type of modes (non-radial versus radial) can also come from the ratio of radial velocity to photometric amplitudes (2 K/ΔV). Radial pulsators such as Cepheids tend to have 2 K/$\Delta V \approx 50$−100 km s^{-1} mag^{-1} while nonradial pulsators tend to have smaller values. Table 5 lists the frequencies in the RV data for which we think we have found a counterpart in the photometric data. The 2 K/ΔV ratio is listed in the last column. All but one mode have 2 K/ΔV in the range of 57−103 consistent with radial pulsators. One mode (f_{v10}/f_{p14}) shows a 2 K/ΔV ratio consistent with nonradial modes. We caution the reader that because the photometric and spectroscopic data were not simultaneous we cannot be sure that the RV amplitude for a mode was the same during the time of the photometric measurements. A more accurate determination of the radial velocity to photometric amplitude would require simultaneous measurements. However, at face value both the frequency spacing of the modes and the values 2 K/ΔV argue in favor of radial modes.

It is not entirely clear what the nature of the low frequency modes seen in both the spectroscopic and photometric data is, but low order radial pulsations may be a prime candidate. The expected frequencies of the fundamental (F) and first 2 harmonics (1H, 2H) for radial pulsations are 1.5, 2 and 2.5 c d^{-1} ($P = 0.67$, 0.5, and 0.4 d) using the pulsation constants of Cox et al. (1972). These are close to f_{v3} (2H) and f_{v14} (F) in the RV data and f_{p1} (2H) and f_{p11} (F) in the MOST data. Using the pulsation constants from Xiong & Deng (2007) which may be more appropriate for cool giants results in a fundamental and first harmonic frequency of 1.67 and 3.22 c d^{-1}, respectively. These also close to the frequencies of f_{v14} and f_{v9} in the RV data and f_{p13} and f_{p8} in the photometry. If these are indeed low order radial modes then it seems that β Gem can excite radial modes over a wide range of orders. We note that the low frequency modes f_{v1} and f_{v5} in the RV and f_{p2} and f_{p7} in the photometry cannot readily be attributed to radial pulsations. However, a detailed pulsational analysis using appropriate stellar models for β Gem are needed to identify properly all detected modes.

Besides radial versus nonradial modes, the lifetime of the modes in K giant stars has also been the subject of discussion in the literature. By fitting Lorentz profiles to the power spectrum of ϵ Oph Barban et al. (2007) derived mode lifetimes of 2.7 days. However, Kallinger et al. (2008) suggested lifetimes of 10 to 20 days and argued that many of the peaks in the broad Lorentz profiles may have actually been independent modes. Photometric data on giant stars obtained by CoRoT indeed confirmed that some K giant stars can have mode lifetimes of tens of days (De Ridder et al. 2009), if not longer. Our excellent fitting of our RV data for β Gem that spans 120 days also suggest the mode lifetimes, at least for this star, are relatively long, or are re-excited on a regular basis.

The main goal of our analysis was to derive the p-mode frequency spacing of β Gem and to combine this with the interferometric stellar radius in order to determine a model independent stellar mass. Our resulting stellar mass of $1.91 \pm 0.09\ M_{\odot}$ is in excellent agreement with the value of $1.96 \pm 0.19\ M_{\odot}$ determined from evolutionary tracks. However, we should note that the mass determination from evolutionary tracks depends critically on the derived stellar parameters. For example, if we use the $T_{\rm eff}$ and [Fe/H] of Allende Prieto et al. (2004) we obtain a stellar mass of $M = 1.47 \pm 0.45\ M_{\odot}$. Thus the actual error in the mass determination from evolutionary tracks is probably much larger than the formal errors using a given set of stellar parameters. The stellar mass derived from the frequency spacing is thus a better determined value since it is independent of $T_{\rm eff}$ and abundance. β Gem is thus one of the few planet hosting stars for which we have an accurate measurement of the stellar mass. The combination of stellar oscillations and interferometric radius determinations can provide a powerful tool for verifying stellar evolution codes using nearby, bright giant stars and to obtain more accurate stellar masses for planet hosting giant stars.

The questions regarding whether β Gem oscillates only in radial modes, whether it can also excite nonradial modes, or what the actual mode lifetimes are all remain open. Unfortunately, our RV data set has several long data gaps and the MOST data length is too short. Long, *uninterrupted* observations are required for this and this can only be done photometrically from space, or spectroscopically from multi-site campaigns or with a dedicated network of telescopes. This star is an ideal target for spectroscopic studies with RV measurements with the proposed SONG network of telescopes (Grundahl et al. 2009) or with high precision photometry using the micro-satellite BRITE-Constellation (Weiss et al. 2008).

Acknowledgements. We thank the referee for useful comments that improved the manuscript. This research has made use of the SIMBAD data base operated at CDS, Strasbourg, France. A.P.H. acknowledges grant HA 3279/5-1 from the Deutsche Forschungsgemeinschaft (DFG). M.Z. acknowledges financial support from DFG grant RE 1664/4-1.

References

Allende Prieto, C., Barklem, P. S., & Lambert, D. L. 2004, A&A, 420, 183
Barban, C., Matthews, J. M. de Ridder, J., et al. 2007, 468, 1033
Baudin, F., Barban, C., Goupil, M. J., et al. 2012, A&A, 538, A73
Buzasi, D., Catanzarite, J., Laher, R., et al. 2000, ApJ, 532, 133
Cox, J. P., King, D., & Stellingwerf, R. 1972, ApJ, 171, 93
da Silva, L., Girardi, L., Pasquini, L., et al. 2006, A&A, 458, 609
De Ridder, J., Barban, C., Carrier, F., et al. 2006, A&A, 448, 689
De Ridder, J., Barban, C., Baudin, F., et al. 2009, Nature, 459, 398
Girardi, L., Bressan, A., Bertelli, G., & Ghiosi, C. 2000, A&AS, 141, 371
Gray, R. O., Corbally, C. J., Garrison, R. F., McFadden, M. T., & Robinson, P. E. 2003, AJ, 126, 2048
Grundahl, F., Christensen-Dalsgaard, J., Arentoft, T., et al. 2009, CoAsT, 158, 345
Hatzes, A. P., & Cochran, W. D. 1993, ApJ, 413, 399
Hatzes, A. P., & Cochran, W. D. 1994, ApJ, 422, 366
Hatzes, A. P., & Zechmeister, M. 2007, ApJ, 670, L37 (HZ07)
Hatzes, A. P., Guenther, E. W., Endl, M., et al. 2005, A&A, 437, 743
Hatzes, A. P., Cochran, W. D., Endl, M., et al. 2006, A&A, 457, 335
Han, I., Lee, B. C., Kim, K. M., et al. 2010, A&A, 509, 24
Johnson, J. A., Fischer, D. A., Marcy, G. W., et al. 2007, ApJ, 785
Jørgensen, B. R., & Lindegren, L. 2005, A&A, 436, 127
Kallinger, T., Guenther, D. B., Weiss, W. W., et al. 2008, CoAst, 153, 84
Kallinger, T., Weiss, W. W., De Ridder, J., Hekker, S., & Barban, C. 2009, ASP Conf. Ser., 404, 307
Kjeldsen, H., & Bedding, T. R. 1995, A&A, 293, 87
Kürster, M., Schmitt, J. H. M. M., Cutispoto, G., & Dennerl, K. 1997, A&A, 320, 831
Lenz, P., & Breger, M. 2004, in IAU Symp. 224, eds. J. Zverko, J. Ziznovsky, S. J. Adelman, & W. Weiss (Cambridge, UK: Cambridge University Press), 786
McWilliam, A. 1990, ApJS, 74, 1075
Mosser, B., Groupil, M. J., Belkacem, K., et al. 2012, A&A, 540, 143
Nordgren, T. E., Sudol, J. J., & Mozurkewich, D. 2001, AJ, 122, 2707
Niedzielski, A., Gozdziewski, K., Wolszczan, A., et al. 2009, ApJ, 693, 276
Reffert, S., Quirrenbach, A., Mitchell, S., et al. 2006, ApJ, 652, 661
Sato, B., Ando, H., Kambe, E., et al. 2003, ApJ, 597, 157
Setiawan, J., Hatzes, A. P., von der Lühe, O., et al. 2003, A&A, 398, 19
Scargle, J. D. 1982, ApJ, 263, 835
Stello, D., Chaplin, W. J., Basu, S., Elsworth, Y., & Bedding, T. R. 2009, MNRAS, 400, 80
Tassoul, M. 1980, ApJS, 43, 469
van Leeuwen, F. 2007, A&A, 474, 653
Walker, G., Matthews, J., Kuschnig, R., et al. 2003, PASP, 115 1023
Weiss, W. W., Moffat, A., & Kudelka, O. 2008, CoAst, 157, 271
Xiong, D. L., & Deng, L. 2007, MNRAS, 378, 1270